7

REACTION KINETICS AND CHARACTERIZATION

UTPAL K. SINGH
Chemical Process R&D, Eli Lilly and Company, Chemical Product R&D, Indianapolis, IN, USA
CHARLES J. ORELLA
Chemical Process Development and Commercialization, Merck & Co., Inc., Rahway, NJ, USA

7.1 INTRODUCTION

Characterization and understanding of reaction kinetics is an important part of chemical development in the pharmaceutical industry. The information gleaned from reaction kinetic studies are used for a range of different applications including process optimization, process safety evaluation, scale sensitivity understanding, and robustness testing. The use of reaction kinetics for each of these applications will be discussed in greater detail below with a particular emphasis on measuring reaction kinetics to probe the effect of scale and the effect of convolution of reaction kinetics with transport limitations.

This chapter focuses on some of the characteristics that make pharmaceutical processing unique from commodity and to a lesser degree from specialty chemicals. The literature has many excellent texts and articles devoted to a wide variety of perspectives on chemical reactions. Generally, these fall in three categories of mechanistic chemistry, reaction kinetics, or reactor design and operation. Far too frequently, these approaches are taken independently, without application of all three categories in a harmonized fashion. We have not recreated the full scope of excellent literature, and recommend the reader make good use of existing literature for chemistry or kinetics with or without reactor design and operation (reaction engineering) [1–6].

Our focus is on several aspects of these perspectives that offer room for increased application and impact by chemists and engineers working to successfully characterize, scale, and optimize chemical reactions within the pharmaceutical industry. The first differentiating feature of reactions within the pharmaceutical industry is the complexity and richness of the chemistry, with multiple reactive moieties present in molecules available for desired and more often undesired reactions. This often creates a barrier between chemists and engineers, which is only overcome by close collaboration to at least partially understand the chemistry and mechanism, the kinetic pathways and rates, and the most desirable reactor design model and operating mode. In order to address this complexity of the chemistry, it is necessary to make measurements that help uncover the underlying mechanisms, kinetic pathways, and rates. We seek to obtain unambiguous data about the reactions, which will bring together chemists and engineers to challenge and agree based on quantitative data.

The second feature that has differentiated the pharmaceutical industry to this point is the use of batch processing for the majority of operations, which results in scale up from the milliliter scale to the cubic meter scale (6 orders of magnitude). Over such a wide range of scale, the rate-limiting step is subject to vary with the scale, which poses challenges for understanding and controlling quality and consistency in the eventual manufacturing. In order to successfully scale up, it's necessary to apply or design the right equipment, and operate in such a manner to understand the rate-limiting step at every scale. For this reason, there needs to be a rational approach to characterizing the chemistry and the equipment used at every scale.

Chemical Engineering in the Pharmaceutical Industry: R&D to Manufacturing Edited by David J. am Ende

This incredible diversity in chemistry that is practiced in the pharmaceutical industry was recently captured by researchers at Pfizer. They reviewed the chemistry that was conducted at Pfizer over the course of 17 years and found that a small number of reaction classes contributed to a large fraction of their portfolio [7]. Better understanding of the mechanistic basis for these reaction classes by the practicing chemical engineer can aid process development by rationalizing and in-some cases predicting the effect of scale on the different reaction pathways. In light of the diversity of the chemistry described above, it is important to note that it is difficult, if not impossible, to make broad generalizations that can apply to the range of different chemistries in practice.

Some commonalities across the range of chemistries can be found from a report by which surveyed 22 different processes comprised of 86 different reactions; and classified them according to overall kinetics as well as homogeneous or heterogeneous nature of the reaction mixture [8]. They found that nearly 75% of the reactions were classified as either rapid or moderate and therefore have potential to be affected by scale. Additionally, a vast majority of the surveyed reactions were heterogeneous in nature due to the presence of multiple phases in the reaction mixture, that is, solids and gases. The combination of the heterogeneous nature of the reaction mixture along with the rapid nature of many of the reactions lends itself to the potential for scale sensitivity thereby underlying the need to understand and characterize reaction kinetics.

Characterization of reaction kinetics requires an understanding of the interplay of the rate of chemical transformation to that of the physical transformation. Scale sensitivity is exhibited when the rates of chemical transformation are faster than that for the physical transformation, that is, mixing, heat input, or removal. This chapter will outline some of the techniques that are available for characterization of chemical transformations as well as physical transformations.

7.2 EXPERIMENTAL APPROACHES

Several different equipment and technologies are available to aid in reaction kinetics measurements and this area is continuously evolving as the levels of automation and analyzer sophistication increases.

7.2.1 Calorimetry

Reaction calorimetry is a versatile and highly effective tool for reaction characterization in the pharmaceutical industry. The technique requires conducting an energy balance around the batch reactor yielding the following

$$MC_p \frac{dT_r}{dt} = UA\left(T_j - T_r\right) + R_{rxn}\Delta H_{rxn} + mC_p(T_{addn} - T_r) \tag{7.1}$$

where M, C_p, UA, T_j, T_r, R_{rxn}, ΔH_{rxn}, T_{addn} are reaction mixture mass, heat capacity of reaction mixture, heat transfer coefficient, jacket temperature, reactor temperature, reaction rate, heat of reaction, and temperature of added stream, respectively. The measurement can be conducted in an isothermal or nonisothermal mode which changes the relevant terms in the equation above. Since this techniques measure the total heat of reaction, it convolutes the heats associated with several chemical processes including heats of mixing, dissolution, crystallization as well as heats associated with all reactions including desired reaction and side reactions. For safety testing, this is ideal since such a measurement allows a lumped measurement of heat associated with all relevant chemical events in the process. For measurement of detailed reaction kinetics requiring deconvolution of different processes, reaction calorimetry offers the advantage of the fact that subtle changes in concentration profiles are magnified in heat flow measurements since the heat flow is directly proportional to the reaction rate. This methodology has been routinely highlighted in the works of Blackmond and coworkers as shown in Figure 7.1, which shows the rate profile during Pd/BINAP catalyzed cross coupling of bromobenzene with *N*-methylpiperazine. Conversion profiles measured using GC measurements (filled symbols) shows a potential inflection point during the first hour of reaction. The heat flow profile, which is effectively the reaction rate at a given time, accentuated this behavior clearly by showing an induction period during the first 100 min of reaction (approximately 50% conversion). This reaction was studied in great detail and systematic analysis has been highlighted in works of Blackmond and coworkers [9–12].

A systematic use of reaction progress kinetic analysis using *in situ* reaction calorimeter has been documented by Blackmond and coworkers; and several review articles articulate this approach is great detail [9, 10].

One important caveat should be applied when measuring rapid reaction kinetics especially when the process kinetics are of the same scale or faster than the equipment time constant, the measured rate constant can significantly vary. Table 7.1 shows a comparison of acetic anhydride hydrolysis from calorimetry with that from literature. As the reaction half-life is shortened to less than 1 min, the difference between the measured reaction rate and that from literature increases. A number of different algorithms are available for deconvoluting the equipment time constant from the measured kinetics [13]; however, this process can, depending on the vendor, be a black box. Nevertheless, these results indicate that reaction calorimetry can adequately measure reaction rates under

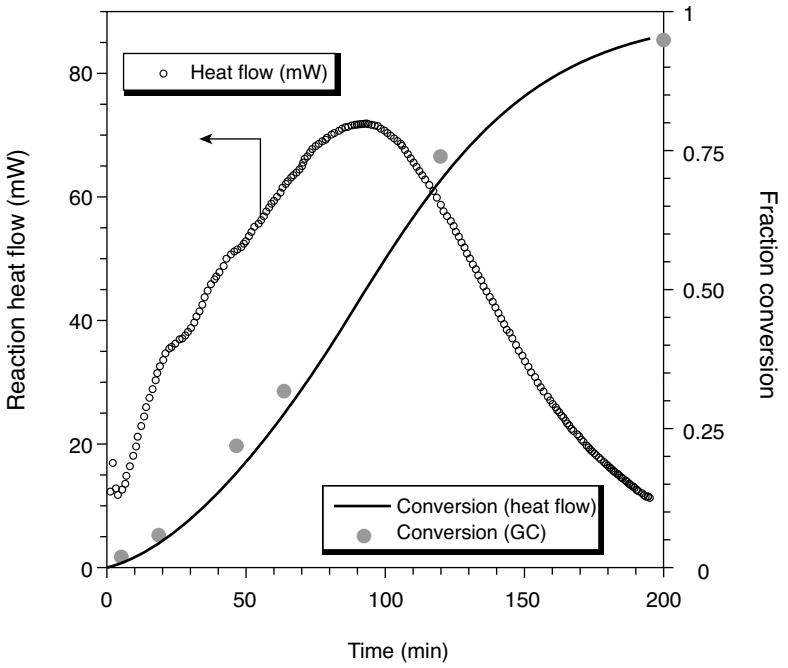

FIGURE 7.1 Reaction heat flow and fraction conversion versus time for the amination of bromobenzene (**1**, 0.71 M) with *N*-methylpiperazine (**2b**, 0.86 M) using NaO*t*Am (1.0 M) as base and a 0.5:1 mixture of $Pd_2(dba)_3$ and BINAP (2 mol% Pd based on [**1**]0) as catalyst. *Source*: Ref. 12.

TABLE 7.1 Comparison of Reaction Kinetics for Acetic Anhydride Hydrolysis Using an Omnical Z3 Calorimeter with that from Literature

Temperature (°C)	k_{obs} (1/s)	k_{lit} (1/s)	Measured Half-Life (s)	Expected Half-Life (s)
55	0.017	0.024	41	29
45	0.012	0.011	58	63
35	0.00585	0.00525	118	132

Source: Ref. 14.

synthetically relevant conditions with half-lives greater than 1 min.

Results from reaction calorimetry are further enhanced when orthogonal techniques are utilized in parallel. One such example of using orthogonal techniques is in the kinetic investigation of heterogeneous catalytic hydrogenation of nitro compounds shown in Scheme 7.1 [15]. The basic reaction network is described in Scheme 7.1.

Hydrogen uptake and reaction calorimetry data are shown in Figure 7.2 [15]; and similar temporal profiles are observed with both hydrogen uptake and reaction calorimetry. Concomitant LC sampling indicated that the zero order kinetics observed during the first 120 min, as evidenced by a flat temporal hydrogen uptake profile, is attributed to hydrogenation of the nitro moiety to the corresponding hydroxyl amine as shown in Scheme 7.2.

Taking the ratio of the two curves shown in Figure 7.2 yields the plot in Figure 7.3, which allow one to deconvolute the energetics for hydrogenation of the hydroxylamine with that to form the amine. The corresponding energetics extracted from the graph is shown in Table 7.2.

Such information and characterization is useful for safety assessment as well as reaction optimization. Understanding of reaction orders and energetics for each pathway in the

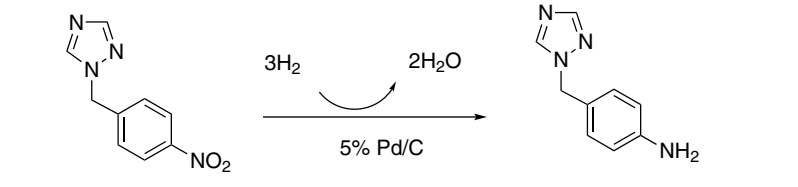

1-(4-Nitrobenzyl)-1,2,4-triazole 1-(4-Aminobenzyl)-1,2,4-triazole

SCHEME 7.1 Hydrogenation of 1-(4-nitrobenzyl)-1,2,4-triazole.

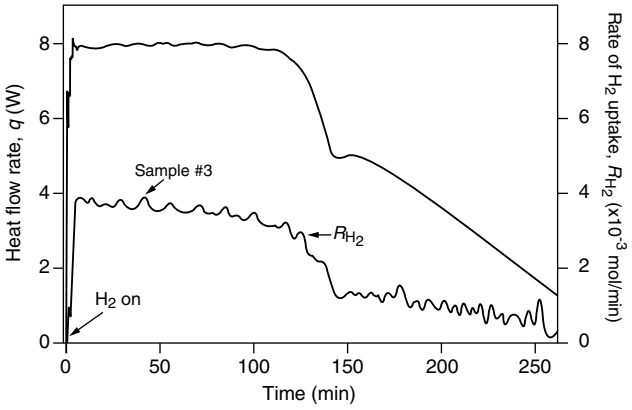

FIGURE 7.2 Temporal hydrogen uptake and reaction calorimetry for hydrogenation shown in Scheme 7.1. *Source*: Ref. 15.

$$\text{Ph-NO}_2 + 2\text{H}_2 \longrightarrow \text{Ph-NHOH} + \text{H}_2\text{O}$$
$$\text{Ph-NHOH} + \text{H}_2 \longrightarrow \text{Ph-NH}_2 + \text{H}_2\text{O}$$

SCHEME 7.2 Stepwise reduction of the nitro moiety.

reaction can be used to understand the operating design space. This example highlights the power of using orthogonal techniques to characterize reaction kinetics. Clearly the use of any one of the analytical techniques alone was not as powerful as the synergy of leveraging online hydrogen uptake, calorimetry, with off-line LC measurements.

Other calorimetry types, especially ARC (Accelerated Rate Calorimetry), are frequently used for process safety evaluation. Several other reviews have been written discussing the details of ARC testing and analysis [16].

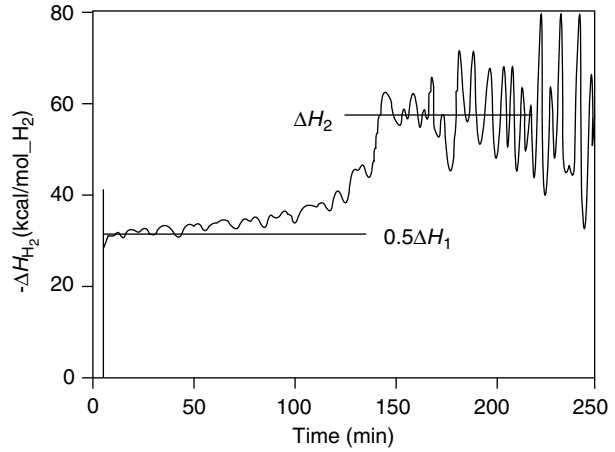

FIGURE 7.3 Ratio of temporal hydrogen uptake and calorimetry to elucidate the energetic of stepwise hydrogenation kinetics. *Source*: Ref. 15.

TABLE 7.2 Stepwise Heat of Hydrogenation of Nitro Group in Scheme 7.1

Hydrogenation Reaction	ΔH (kcal/mol)
$\text{Ph-NO}_2 + 2\text{H}_2 \rightarrow \text{Ph-NHOH} + \text{H}_2\text{O}$	−65
$\text{Ph-NHOH} + \text{H}_2 \rightarrow \text{Ph-NH}_2 + \text{H}_2\text{O}$	−58

7.2.2 Nonmolecule Specific Measurement

As mentioned above, physical measurements during the process can also serve as a means to track reaction progress and characterize reaction kinetics. These physical measurements can take many forms; however, temperature, gas flow, and pH are three more common measurements to characterize reactions. As mentioned with calorimetry, such measurements lump several different chemical events; and hence caution must be exercised for complex reaction systems.

Gas uptake measurements are particularly useful for multiphasic reaction such as hydrogenation as was outlined in the example above. As with calorimetry, care must be taken to ensure that the observed gas uptake measurement is correlated with the desired chemical transformation that is being tracked. Often times, side reactions such as over-reduction of desired products or catalyst reduction can mask the details of the chemical transformation that is to be tracked. Conversely, gas evolution measurements can also be used to track progress. This is frequently the case for decarboxylation reactions in which CO_2 evolutions can be used as a means to monitor and characterize decarboxylation kinetics.

Temperatures has been used for decades to track reaction progress; and it sometimes gets mistakenly neglected in favor of more complicated online sensors that are currently available. Tracking reaction progress with temperature, especially for exothermic reactions, that is, Grignards, are effective. Figure 7.4 shows the tracking of reaction progress at a 200 gallon scale during a benzyl Grignard formation. The initiation is evident during the time span of 150–200 min followed by formation of Grignard in a feed-limited manner up to approximately 330 min. The use of these physical measurements allow characterization and estimation of reaction rate constants both on lab and pilot plant scale which, in turn, can be used to understand scale sensitivity as will be discussed in subsequent sections.

7.2.3 Online Spectroscopy

The past 10 years has seen significant development of online technologies that have proven very effective for reaction characterization and measurement of reaction kinetics. While several online spectroscopic techniques are available, mid-IR, Raman, and NIR have proved to be the most valuable. A detailed review of each of these technologies is

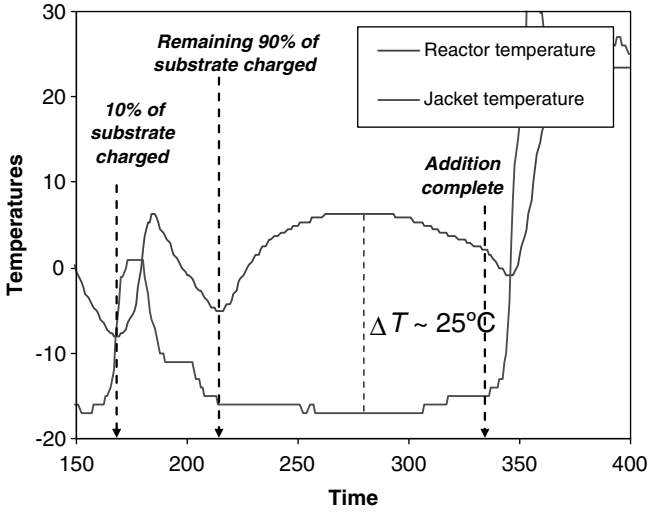

FIGURE 7.4 Reactor and jacket temperature profiles during the formation of a Grignard in a 200 gallon reactor. Both the initiation and the postinitiation reactive regimes are shown in the figure.

beyond the scope of this chapter; and several reviews have been written on this subject matter [17]. These technologies have been used routinely by the practicing chemist and engineering to extract detailed reaction kinetics and mechanistic information.

During the past few years, ReactNMR has also proved to be a valuable resource in understanding and characterizing reactions. *In situ* NMR has been widely used in academic environments; and lately, *in situ* NMR is also being used in industrial settings for probing reaction kinetics under synthetically relevant conditions. Use of different types of NMR (different nucleus) allows specific information to be gleaned that would otherwise not have been possible by conventional methods. This area will continue to garner more attention as additional applications show greater utility of this technique.

The above technologies are highly effective at measuring a vast majority of processes in the pharmaceutical industry; however, certain applications, such those requiring extreme reaction conditions and rapid kinetics, require specialized equipment such as stop-flow apparatus or tubular reactors.

7.2.4 Off-Line Concentration Measurements

There are several online and physical measurements that can be used to track reaction progress, as mentioned above; however, off-line concentration samples are a powerful means to track reaction progress especially with complex reaction networks and when tracking trace levels of impurities less than 0.5%. Newer technologies are being offered to allow online HPLC measurements that circumvent the time and discrepancies associated with manual off-line sampling. Sampling a minimum of 5–10 points across the reaction gives qualitative data regarding the overall reaction kinetics. Because of the separation capability and sensitivity of HPLC analysis applied to such samples, the kinetics of minor and major pathways leading to low level impurities as well as desired intermediates and products can be followed in this manner. In order to generate a richer set of data for quantitative analysis, more frequent sampling is required. This can be accomplished by means of integral data for concentrations of the major species using FTIR, or online or at-line HPLC with sampling taken at intervals of about 2–4% conversion. Recent developments in online LC have been reported in the open literature [18].

7.3 REACTION MODELING

Developing a model requires transformation of a reaction system into a discrete set of descriptions or elementary steps. Models of reaction systems can be developed in a number of different ways. Depending on the application, models can simply be a scale-down version of a pilot or commercial equipment that can be used to predict full-scale performance from laboratory measurements. Alternatively, models can be mathematical in nature in the form of dimensionless parameters or kinetics rate expressions that, when solved, can be used to predict performance. Regardless of the path chosen, models are developed to simplify and explain/rationalize an often complicated system into the most important/relevant elementary steps or rate-determining steps. Experimental data can be generated to test various steps. In such a way, the model guides the experiments, and the data from such experiments is used to support or refute the model. This allows a refining process for the model, which reflects the building of knowledge of the process. Accurate development and utilization of models enables us to have a high degree of confidence of the performance at different scales in batch processing or to apply the best design of a reactor configuration, be it batch or continuous mode. The model is an end goal, but is also helpful to the development of knowledge for any reaction system. As soon as a first draft of a model exists, it can be challenged with experimental data that helps improve or validate the draft of the current model.

Building a model requires measurements that "profile" the reaction from start to final conversion using any one or several techniques outlined above. This gives richer information for analysis than by simply analyzing the final conversion and selectivity or yield. This profiling of the reaction should capture concentration data of reagents, intermediates, and products plus selectivity for by-products along with direct measurements of the rate of reaction. Concentration-based data represent "integral" data, in that they are a direct measure of conversion, which comes from integration of the reaction rate, r.

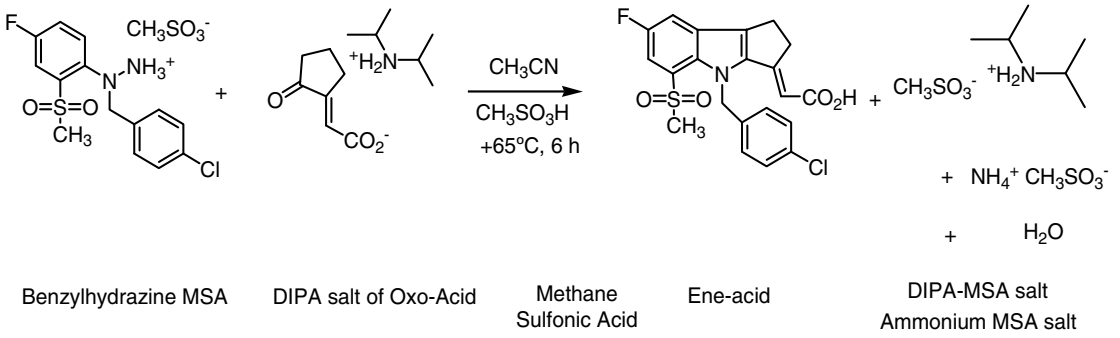

SCHEME 7.3 Example of Fisher indole reaction.

$$X = C/C_0 = \int_0^t (r)dt \tag{7.2}$$

Typically, samples are taken for off-line analysis that provides concentration data by HPLC, GC, FTIR, or equivalent methods, and the samples are taken at intervals of 5–20% conversion. This means that the frequency is a strong function of the half-life of the reaction(s).

Once the profiling data is obtained, it is often times necessary to visualize the data in different ways to characterize reaction kinetics. This has been done routinely for several catalyzed processes by Blackmond and coworkers. The example below adapts this technique for a Fisher indole reaction to understand the interplay of reaction kinetics with solid–liquid mass transfer (Scheme 7.3).

The Fisher indole reaction is expected to proceed through the hydrazone intermediate which exists a slurry with a solubility of 27 mg/mL before strong acid drives the cyclization to close the pyrrole ring and form the bicyclic indole as shown in Scheme 7.4 [19].

Small-scale experiments in a microcalorimeter along with RC-1 calorimeter were carried out to measure the reaction kinetics, with reaction calorimetry and off-line HPLC used to follow reaction progress. Multiple small (0.15 equiv) injections of methane sulfonic acid (MSA) was introduced into a slurry of hydrazone. Figure 7.5 shows calorimetry data modified to show the reaction rate data as a function of hydrazone concentration. This plot was obtained by integrating the heat flow data; and the conversion (or fractional heat evolution) was used to determine the hydrazone concentration during the course of the reaction. Each injection of MSA can be thought of and analyzed as an individual batch reaction. In contrast to conventional plots, the start of the reaction is shown on the right-hand side with higher concentrations of hydrazone. Reaction progresses by hydrazone consumption and movement to the left of the graph. Each peak observed in Figure 7.5 is due to an identical spike of MSA; and, as a result, the MSA concentration at the start of each peak is constant but the hydrazone concentration at the start of each peak is different allowing calculation of the reaction order in hydrazone during the course of the reaction.

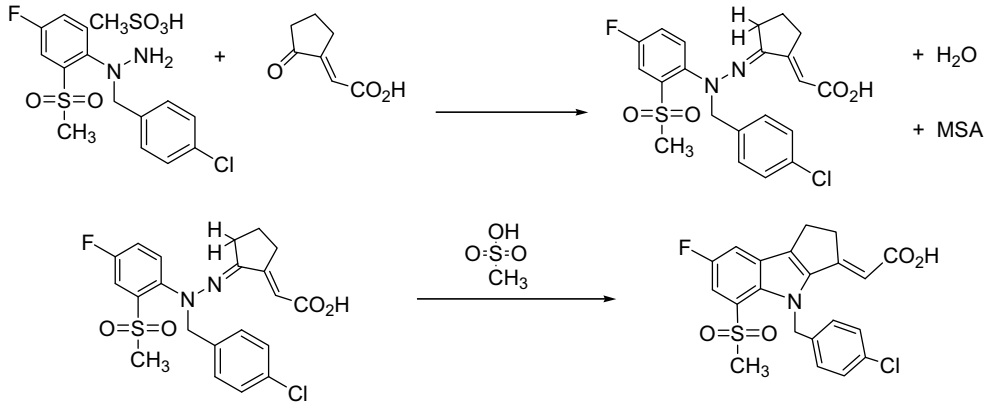

SCHEME 7.4 Proposed pathway for the Fisher indole reaction of Scheme 7.3.

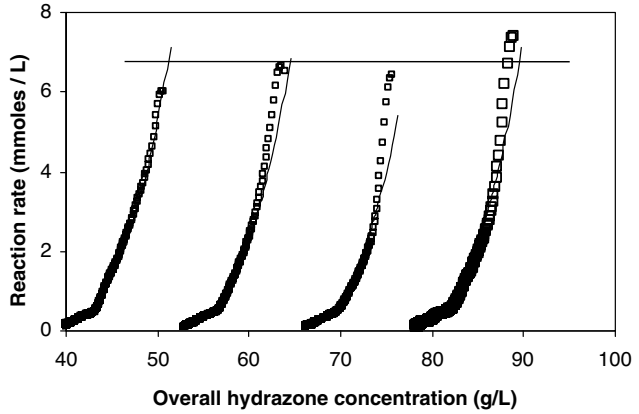

FIGURE 7.5 Rate of Fisher indole reaction as a function of overall hydrazone concentration.

Similarly, during the course of each spike, the MSA is effectively completely depleted whereas the hydrazone concentration would be expected to change little if at all allowing calculation of the order in MSA. The shape including slope and curvature of all four injections are nearly superimposable as shown in Figure 7.6 which shows the same data plotted as a function of MSA concentration. These results indicate that the order in MSA is not changing during the course of the reaction.

The combination of the results in Figures 7.5 and 7.6 indicate that the overall reaction rate is zero order in initial hydrazone concentration as shown by the solid line in Figure 7.5. Additionally, the reaction exhibits an overall third order behavior when plotted as a function of MSA concentration as shown in Figure 7.6 (solid line represents rate profile expected from third order kinetics). The initial zero order kinetics in hydrazone is consistent with the hydrazone being a slurry and the reaction kinetics being

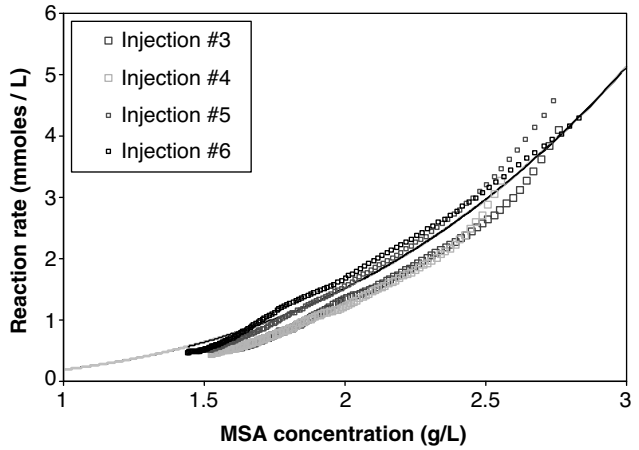

FIGURE 7.6 Rate of Fisher indole reaction as a function of the MSA concentration.

solubility limited in hydrazone. It was difficult to understand the chemical significance of the third order kinetics especially in the context of mechanistic data in the literature [19].

To better understand the underlying mechanism and effect of physical processes such as dissolution kinetics, the solids in the reaction mixture were filtered off and an identical study was conducted under homogeneous conditions using the dissolved hydrazone (saturated with a solubility of 27 mg/mL) in the filtrate; and the results are shown in Figure 7.7a and b. These results indicate a near first order dependence of reaction kinetics on hydrazone concentration and second order dependence on MSA concentration.

In the context of these results, the unusual third order kinetics in Figure 7.6 can be rationalized. The initial rate at the beginning of each MSA spike in Figure 7.5 indicated zero order kinetics in hydrazone since sufficient time was allowed for dissolution and equilibration resulting in identical solution phase concentration of hydrazone at the start of each peak in Figure 7.5. In contrast, first order kinetics with respect of hydrazone concentration was observed during the course of the reaction (each spike in Figure 7.7) since the dissolution rate was slower than the reaction rate resulting in a decrease in hydrazone concentration in each spike. As a result, the overall third order kinetics observed in Figure 7.6 is actually a convolution of second order dependency on MSA concentration and first order dependency on hydrazone concentration.

Independent dissolution rate measurements confirmed that the dissolution kinetics were occurring under the same timescale as that for the reaction. Understanding of this behavior led to a better phenomenological understanding and characterization of the reaction. This was particularly important since the solubility limited process (for both the starting material and the product) results in a slurry to slurry conversion resulting in significant occlusion of the starting material in the product depending on the addition mode and rate utilized.

As mentioned earlier, it is imperative when using online techniques such calorimetry or various spectroscopic tools to profile kinetics that one use orthogonal techniques to ensure the absence of artifacts affecting the measurements and hence the final conclusions. To that extent, Figure 7.8 indicates a comparison of the kinetic profile for hydrazone concentration as inferred from calorimetric measurements and that through quantitative IR measurements. Excellent agreement of data from different analytical techniques adds more credence to the measured kinetics.

The above example highlights an important point that will be examined in more detail in sections to follow, that is, convolution of reaction kinetics with physical rate processes. The next two examples highlight the importance of understanding the dynamics of reaction progress and the challenges associated with understanding a complicated reaction network with multiple pathways and by-products and

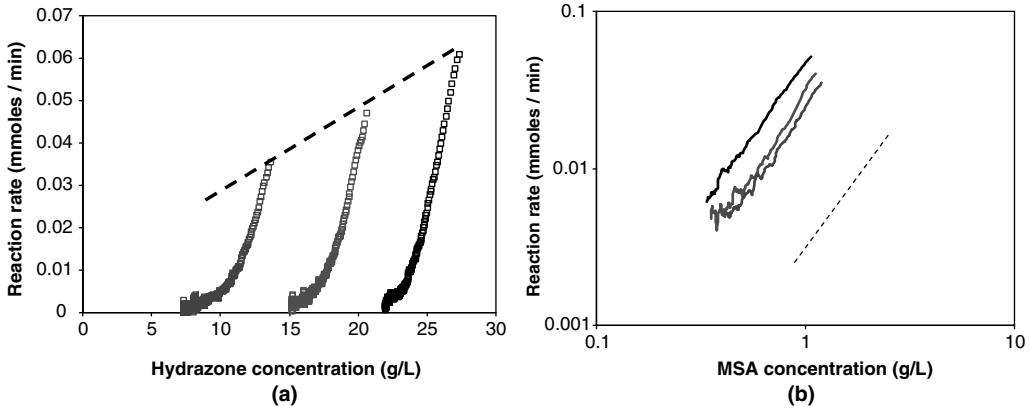

FIGURE 7.7 Plot of reaction rate as a function of (a) hydrazone and (b) MSA concentrations. Dashed lines in a and b represent first and second order curves, respectively.

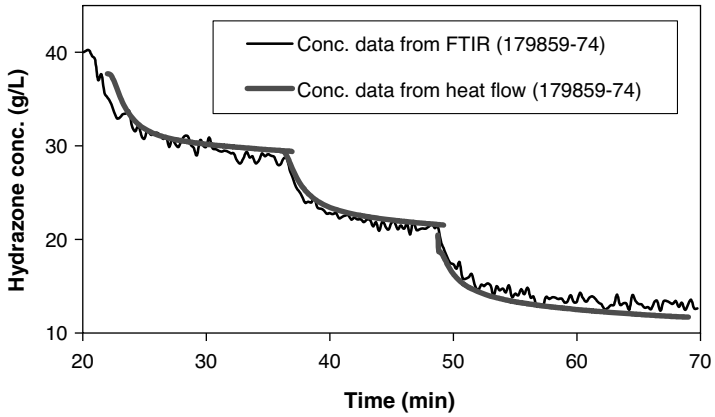

FIGURE 7.8 Comparison of temporal concentration profile obtained from heat flow and IR measurements.

changes in rate-determining step during the course of the reaction.

Let us start with an example from the literature for hydrogenation of ethyl pyruvate using modified Pt catalysts (Scheme 7.5) [20].

This reaction has been studied extensively in the literature to fully characterize the mechanism for enantioselective hydrogenation. The mechanistic understanding was linked to various reaction parameters including, but not limited to, solvent properties, modifier levels and interactions, and

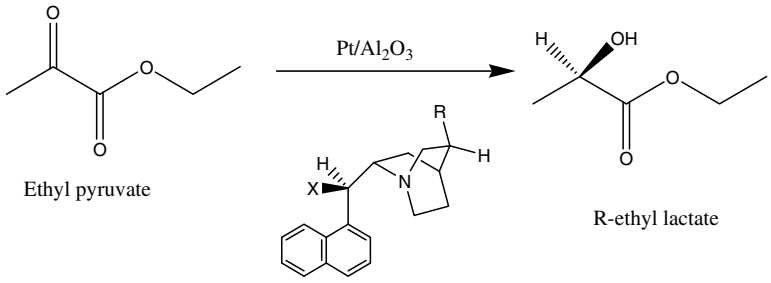

	R	X
Cinchonidine	CH2CH	OH
Dihydrocinchonidine	CH3CH2	OH

SCHEME 7.5 Scheme for enantioselective reduction of ethyl pyruvate via heterogeneous catalysis.

catalyst dispersion and properties; and have helped the long-term strategic understanding. The effect of hydrogen transfer from the gas phase to the liquid phase significantly affects reaction kinetics. To that extent, Sun and coworkers examined the kinetics of the reaction and characterized the rate of hydrogen consumption as follows:

$$\frac{d[H_2]}{dt} = k_L a \times ([H_2]^{sat} - [H_2]) - f\{[H_2], [\text{catalyst}], [\text{substrate}]\} \tag{7.3}$$

where $k_L a$, $[H_2]^{sat}$, $[H_2]$, and $f([H_2], [\text{catalyst}], [\text{substrate}])$ are mass transfer constant from gas phase to liquid phase, equilibrium concentration of hydrogen, hydrogen concentration at a given time, and intrinsic kinetic rate expression, respectively. Measurement of the mass transfer constant along with equilibrium hydrogen solubility and the kinetic rate expression allows one to numerically integrate the above expression to determine the hydrogen concentration during the course of the reaction. To that extent, the reaction rate was measured and the corresponding hydrogen concentration calculated under synthetically relevant conditions and the results are shown in Figure 7.9. Interestingly, there are two regimes evident in the kinetic profile. In the first regime, reaction kinetics is mass transfer limited. However, there is shift in the rate-determining step as the substrate is consumed and the intrinsic reaction kinetics slows sufficiently to become slower than the rate of hydrogen transfer from gas to liquid phase.

The shift in the rate-determining step is also associated with a shift in the selectivity as shown in Figure 7.9b [20]. The plot of cumulative selectivity (defined below) shows little to no change associated with the change in the rate-determining step; however, plotting the incremental selectivity (defined below) shows a marked change in incremental ee upon a change in the rate-determining step.

$$\text{Cumulative selectivity} = \frac{[R]-[S]}{[R]+[S]} \times 100 \tag{7.4}$$

$$\text{Incremental selectivity} = \frac{R_R - R_S}{R_R + R_S} \times 100 \tag{7.5}$$

[R], [S], R_R, and R_S are concentrations of R-enantiomer, S-enantiomer, and rates of formation of R- and S-enantiomers, respectively. The primary difference between the two modes of measuring selectivity is that the subtle changes in product distribution are masked and averaged out in the cumulative selectivity calculation whereas the incremental selectivity highlights incremental changes within two time points.

When modeling reaction kinetics, it must be understood that several competing reaction and equilibrium pathways can combine to yield complex nonintutive reaction kinetics. To this extent, apparent non-Arrhenius type behavior has been documented in literature in the form of activity minimum and maximum. Activity maximum has been observed during gas phase hydrogenation of benzene under initial rate conditions over supported transition metal catalysts; and the results have been rationalized by a conventional Langmuir–Hinshelwood mechanism for heterogeneous catalysis in which the increasing rate of elementary reaction steps

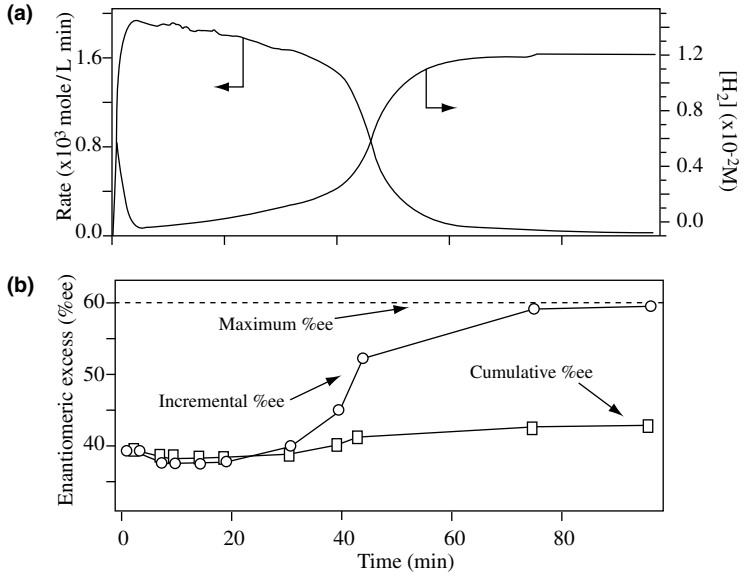

FIGURE 7.9 Plot of the kinetics of ethyl pyruvate hydrogenation. (a) Plot of reaction rate and solution phase hydrogen concentration; and (b) concomitant product distribution calculated during cumulative and incremental selectivities. *Source*: Ref. 20.

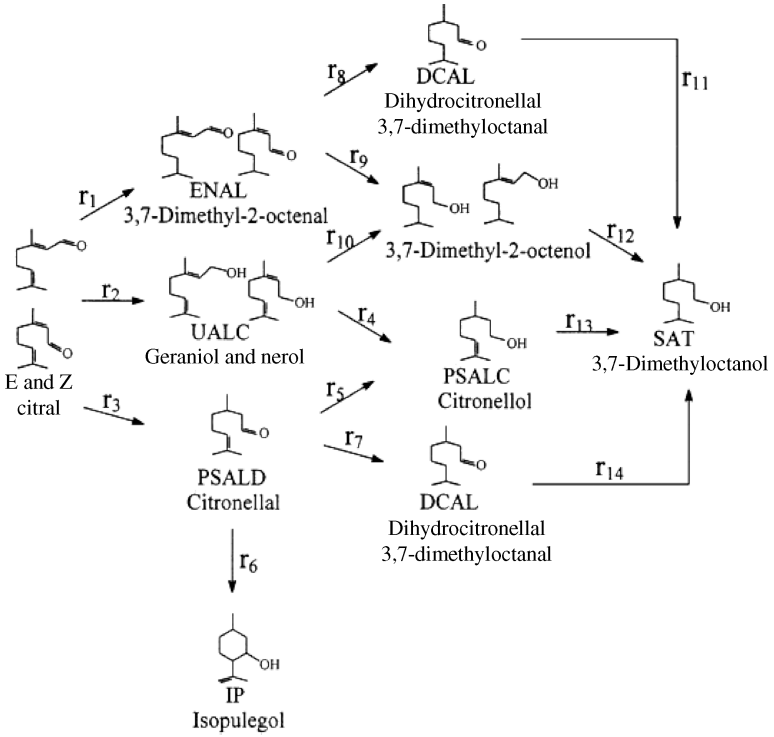

SCHEME 7.6 Reaction network for citral hydrogenation over supported Pt catalysts.

competes with decreasing equilibrium constant with increasing temperature. The opposing trends for these two parameters leads to an observation in which the reaction rate increases to a certain temperature after which the rate decreases with increasing temperature due to decreasing surface coverage of the substrate from decreasing adsorption equilibrium constant [21, 22].

Similarly, activity minimum has been observed during liquid phase citral hydrogenation over supported Pt catalysts [23]. The unusual behavior was rationalized by detailing a concurrent catalyst deactivation pathway occurring simultaneously with the reaction. The overall reaction pathway is shown in Scheme 7.6.

Focusing on pathways r_1, r_2, r_3, and r_5 and assuming that each of these pathways occurs with a similar sequence of elementary steps as outline below. The elementary steps were assumed to include preequilibrated dissociative adsorption of hydrogen and addition of the second hydrogen atom to the unsaturated moiety as the rate-determining step as shown in Scheme 7.7.

The corresponding deactivation pathway was described as follows, in the which the unsaturated alcohol (geraniol) adsorbs on the catalyst surface to make a metal-alkoxy species which then decomposes to form adsorbed CO. The adsorbed CO then desorbs off the catalyst surface with a rate constant k_D as shown in Scheme 7.8.

The rate expression has been derived in detail before [23] with the following result:

$$r_i = \frac{k'K'P_{H_2}C_{org}(1-\theta_{CO})^2}{(1+K_{citral}C_{citral})^2} \tag{7.6}$$

where θ_{CO} is the surface coverage of adsorbed CO and is defined by the following differential equation:

$$\frac{d\theta_{CO}}{et} = k'_{CO}C_{UALC}\theta_S^2 - k_D\theta_{CO} \tag{7.7}$$

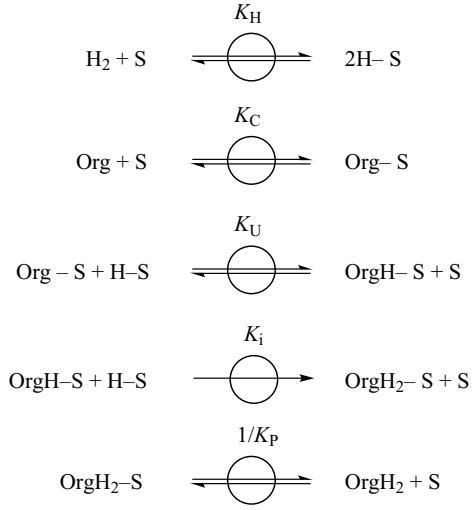

SCHEME 7.7 Elementary steps for hydrogenation of citral.

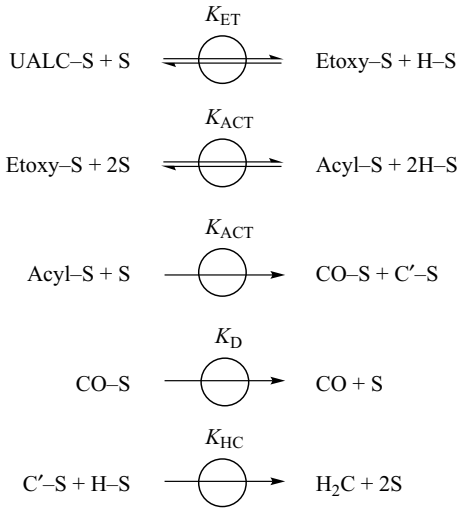

SCHEME 7.8 Elementary steps for decomposition of geraniol to CO.

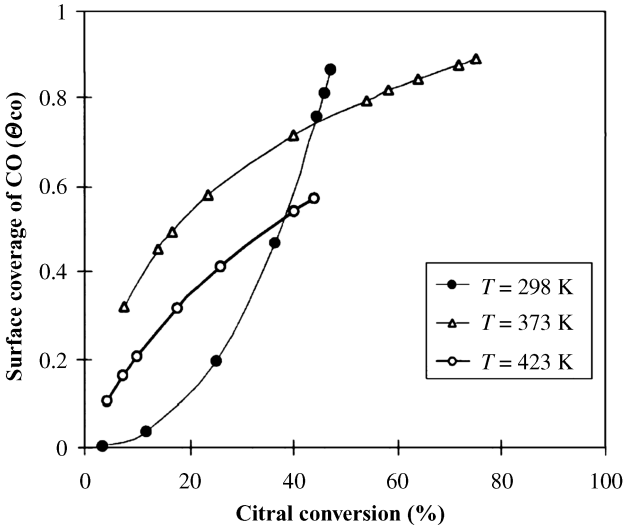

FIGURE 7.11 Calculated surface coverage of CO on supported Pt catalysts under synthetically relevant conditions during citral hydrogenation. *Source*: Ref. 23.

Representing the rate of CO formation via decomposition of the unsaturated alcohol (UALC) and subsequent desorption of CO from the catalyst surface. This deactivation pathway led to formation of CO, which poisoned the catalyst surface. Increasing the reaction rate led to increasing rate of catalyst deactivation and hence a reduction in rate with increasing temperature. After a certain critical temperature, CO starts to desorb off the catalyst surface leading to conventional Arrhenius-like behavior. The correlation of the model with experimental data is shown in Figure 7.10.

Measurement and quantification of the surface species in a solid–liquid interface for polycrystalline metal surfaces can be challenging. Kinetic modeling allows a means to understand the relative abundance of different reactive species and changes in the population of these species under different reaction conditions. For the case of citral hydrogenation, kinetic modeling was used to calculate the surface coverage of CO as shown in Figure 7.11. These relative trends in the surface coverage of CO with changes in temperature are consistent with the unusual trends in temperature that was described above.

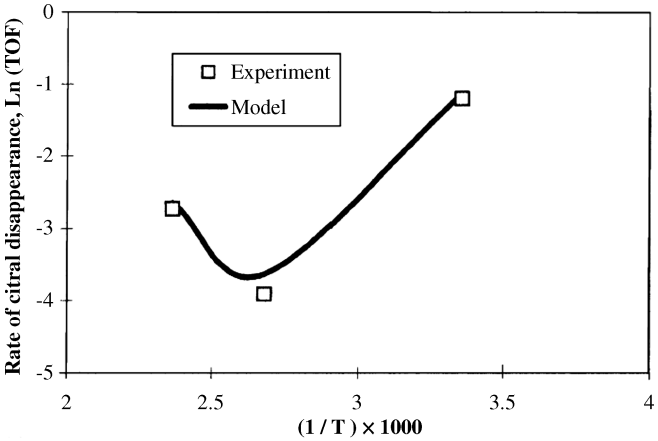

FIGURE 7.10 Comparison of model and experimental data for citral hydrogenation over supported Pt catalysts. H_2 (20 atm) and 1 M citral in hexane. Only the integral data is shown in the figure; however, actual curve fitting required regressing integral data at each temperature point shown. *Source*: Ref. 24.

Nonlinear regression of the model to the measured data allowed estimation of the adsorption equilibrium constant for the substrate along with the enthalpy and entropy of adsorption as well as the corresponding activation energy for the CO formation. Simply fitting of the data to a model is not justification alone for the validity of the model. Orthogonal techniques and independent measurements are necessary to add credibility to the results of curve fitting. Additionally, thermodynamic consistency of the fitted parameters should also be investigated. The standard states for the enthalpy and entropy of adsorption extracted from the temperature dependency of the adsorption equilibrium constant can be changed as shown in literature [23–25]; and the corresponding values have to satisfy additional thermodynamic constraints to ensure validity of the model and the nonlinear regression. For heterogeneous catalytic applications, two constraints have been discussed in the literature:

$$0 < \left|\Delta S^0_{ad}\right| < S^0_g \tag{7.8}$$

$$10 < \left|\Delta S^0_{ad}\right| < 12 - 0.0014(\Delta H^0_{ad}) \tag{7.9}$$

in which ΔS_{ad}, ΔH_{ad}, and S_g are the entropy of adsorption, enthalpy of adsorption, and standard entropy of the gas, respectively [26–28]. The constraint in equation 7.8 is

stringent whereas that in equation 7.9 is a guideline suggested by Boudart and Vannice similar guidelines for elementary reactions in solutions have been detailed by Laidler [29].

7.4 SCALE SENSITIVITY ASSESSMENT

One of the areas where chemical engineers can have significant impact is in the area of understanding the effect of scale on reaction kinetics. To that extent, it is important to understand the relevant rate processes including that for chemical and physical processes. Use of dimensionless parameters can be especially helpful in this manner in understanding the relevant scale-up parameters. A thorough listing of the complete dimensionless parameters is outside the scope of this chapter; however, one parameter that deserves special attention is a variation of the classical Damkohler number. For the purposes of pharmaceutical process development Damkohler number can be applied as follows:

$$Da = \frac{\text{timescale for physical processes}}{\text{timescale for chemical transformation}} \qquad (7.10)$$

In which the rate of physical processes can include just about any process including those associated with mass transfer such as liquid–liquid mixing, gas absorption, gas desorption, solid suspension, as well as heat transfer including rate of heat generation, heat input/removal. Most, if not all, scale sensitivities can be understood in the context of the apparent Damkohler number. In general, no scale-sensitivities would be expected when the rate of the chemical transformation is slower than that for the physical process. In contrast, scale sensitivities are observed when the rate of physical process is slower than that for chemical transformations.

The above statement holds not only for the desired reaction pathway but also for all other chemical pathways that may result in impurity formation. One example of this behavior was the debenzylation of a fumarate salt of an amine to give the corresponding succinate salt of the secondary amine as shown in Scheme 7.9.

The hydrogenation process involves initial reduction of the fumaric acid to succinic acid followed by debenzylation to form the corresponding secondary amine succinate salt. The reaction rate profiles as function of hydrogen pressure is shown in Figure 7.12. These results along with concomitant sampling clearly indicate a positive order dependence of rate

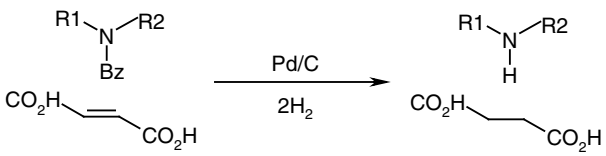

SCHEME 7.9 Debenzylation and corresponding fumaric acid reduction.

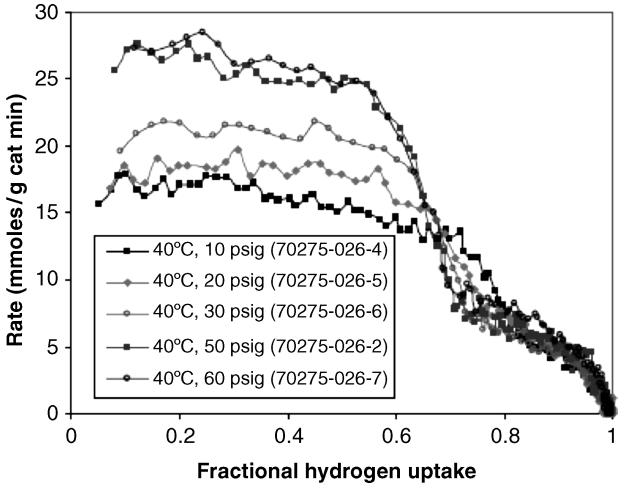

FIGURE 7.12 Temporal rate profile for concomitant debenzylation and fumaric acid reduction over Pd/C for reaction in Scheme 7.10.

of fumaric acid reduction on hydrogen pressure compared to a zero-order dependence for debenzylation. Hydrogen starvation resulted in significant decrease in the rate of fumaric acid reduction with little or no effect on the rate of debenzylation resulting in accumulation of the fumaric acid in the presence of a secondary amine thereby increasing the propensity for the formation of the Michael adduct as described in Scheme 7.10.

For such a process, the Damkohler number is defined as follows:

$$Da = \frac{\text{rate of fumaric acid hydrogenation}}{\text{rate of hydrogen transfer from gas phase to liquid phase}} \qquad (7.11)$$

When the $Da < 1$, the rate of hydrogen transfer from the gas phase to liquid phase is rapid compared to fumaric acid reduction and, as a result, its hydrogenation occurs rapidly. When $Da > 1$, the rate of hydrogen transfer is slower than the rate for fumaric acid reduction; and, as a result, the rate of fumaric acid reduction is slowed to the point that subsequent debenzylation can occur simultaneously thereby allowing the deprotected secondary amine to react with the fumaric acid to form the Michael adduct.

The physical process described in Damkohler expression above is usually related to some aspect of heat and mass transfer of the reactor process. In the case of exothermic reactions, the Damkohler number is expressed as the rate of

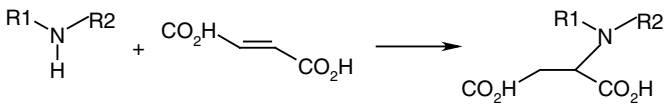

SCHEME 7.10 Michael adduct formation reaction.

heat formation to the heat removal by jacket services. In some cases, the rate of physical process is the rate of the relevant mixing mechanism to that for the reaction rate. Often times deconvoluting chemical and physical processes can be difficult and a more fundamental understanding of the relevant heat/mass transfer and chemical transformation is needed to understand the effect of scale.

It is difficult to make broad generalizations regarding how to measure and characterize reaction kinetics due to diversity of chemistry and the widely varying and highly complex chemical pathways that are known to occur especially when one focuses on pathways that lead to formation of impurities of the order of 0.1% (see discussion above on reaction optimization). Generalizations regarding the characterization of the relevant physical process can be made. To that extent, three relevant mass transfer processes will be discussed.

7.5 SOLID–LIQUID TRANSPORT

In many industrial applications, reactions involve reagents, catalysts, or intermediates that are heterogeneous in nature. In these cases, solid–liquid transport effects may need to be characterized and understood. In such a case, there are multiple ways to model the observed reaction. To do so, it is necessary to understand the rate of the solid–liquid transport, as well as the rate of the intrinsic chemical reactions. Deconvoluting the intrinsic rate of chemical kinetics from solid–liquid mass transfer rates can be complex. Calculations to estimate the transport from particles in heterogeneous reactions have been outlined by Zwietering [30]. Specifically, experimental data and mathematical correlations indicate that the rate of mass transfer changes appreciably up to the "just suspend" point for particles, at which point the particles no longer form a layer at the bottom of the vessel. Further increases in mixing intensity once solids have already been suspended give only marginal increases in the mass transport [31]. While this guidance provides an effective rule of thumb for guiding process development, detailed kinetic studies are occasionally necessary in order to decouple the different rate processes and obtain quantitative expressions for the intrinsic transport and reaction rates.

There are several ways to approach decoupling the transport rate from the chemical kinetics. A number of different mass transfer correlations are available in the literature [32]; and the different formulations can be used to estimate the rate of mass transfer across the solid–liquid interface and compare with the corresponding intrinsic reaction rate constant using a Damkohler number type approach articulated above. *A priori* determination of the mass transfer constant from correlations can be unreliable if one does not pay attention to the appropriate assumptions involved. Numerous correlations have been reported in the literature looking at functional relationship between the dimensional groups of Sherwood number, Reynolds number, and Schmidt number. Each of these dimensionless parameters is defined below

$$Re = \frac{\rho u d_p}{\mu}\,(\text{particle basis}) \quad \text{or} \quad Re = \frac{\rho u d_T}{\mu}\,(\text{impeller basis}) \tag{7.12}$$

$$Sc = \frac{\mu/\rho}{D} \tag{7.13}$$

$$Sh = \frac{k_d d_p}{D} \tag{7.14}$$

The term ρ represents the fluid density, u is the velocity, d is the characteristic length scale for particles (p) or turbine (T), μ is the fluid viscosity, D is the diffusion coefficient for the substrate or reagent of interest, and k_d is the mass transfer coefficient In general, these correlations have a functional form as shown below.

$$Sc = kRe^x Sc^y \tag{7.15}$$

where the constants k, x, and y vary depending on the system under consideration. One of the issues that arises when utilizing this correlation is the formulation of the Reynolds number. A number of different modified particles Reynolds number expressions are shown in the literature and care should be exercised to ensure that the assumptions are known and that the correct correlations are utilized [31]. Many studies have been carried out and published on the mass transfer to particles. Most studies are for transport of particles in stirred tanks although transfer in pipes was reported by Harriott [33–39]. It should be noted that there is wide spread dissolution measurements upon which these correlations have been made, and so the use of such correlations introduces a measurable level of uncertainty when applied in a new scenario.

Rather than using the correlations, it is preferable to explicitly measure the mass transfer constant across the solid–liquid interface using dissolution measurements. Several model systems have been evaluated and reviewed. This approach allows a direct measurement of the rate constant to compare with the corresponding reaction rate constant.

Alternatively, one could use the formulation of the rate equation that combines the rate constant for solid–liquid transport with the intrinsic reaction rate constant; and then use the relative activation energies as a means to deconvolute transport and reaction limited regimes. For a first order reaction, the rate expression that combines reaction rate constant and mass transfer across the boundary layer can be written as follows [40–41]:

$$R_G = \frac{k_d k_r}{k_r(1-w_\infty) + k_d} C \tag{7.16}$$

$$\mathrm{HCL} + \mathrm{NaOH} \xrightarrow{k_1} \mathrm{NaCl} + \mathrm{H_2O}$$

$$\mathrm{DMP} + \mathrm{HCL} + \mathrm{H_2O} \xrightarrow{k_2} 2\mathrm{MeOH} + \mathrm{Acetone} + \mathrm{HCL}$$

SCHEME 7.11 Reaction network for the fourth Bourne reaction. DMP stands for 2,2-dimethoxypropane.

where k_d and k_r are the rate constants for transport across the solid–liquid interface. In cases, where the mass transfer across the solid to liquid interface is rapid, that is, $k_d \gg k_r$ then the rate expression simplifies to $R = k_r C$ and chemical kinetics are rate controlling. In cases, where the mass transfer across the solid–liquid interface is slow, that is, $k_d \ll k_r$ then the rate expression simplifies to $R = k_d C$ and mass transfer across the boundary layer is the rate-limiting step.

The temperature dependency of the rate constant k_r and k_d allows deconvolution of the chemical kinetics with mass transfer kinetics. The influence of temperature on the transport rate is primarily through its influence on viscosity and/or diffusion coefficients. There is only a modest effect of temperature on these variables; and, as a result, the transport rates typically exhibit a weak dependency with temperature, that is, a low activation energy. As a rule of thumb, activation energies for transport limited processes are typically of the order of 10–20 kJ/mole compared to 40–60 kJ/mole for reaction processes. It should be stressed that this is a rule of thumb and some exceptions do exist in the literature especially in the context of the unusual temperature dependencies that were articulated in the section above. Such a technique has been routinely used in heterogeneous catalytic systems and has also been applied to crystallization processes [42].

7.6 LIQUID–LIQUID TRANSPORT

There have been several reviews written documenting the effect of liquid–liquid mixing in pharmaceutical applications; and a detailed discussion on the mechanistic aspects of liquid–liquid mixing is outside the scope of this review [43]. The focus instead will be on the convolution of reaction kinetics with liquid–liquid mixing either in a miscible system or in immiscible systems.

One of the powerful tools in characterizing liquid–liquid mixing is the Bourne reaction. Several Bourne reactions exist but the fundamental principle of the reactions is a competition between a sequence of slow and fast reactions. In the event of perfect mixings, only the fast reaction occurs; and the extent to which the slow reaction occurs is a measure of poor mixing. The known rate constants of the Bourne reaction can be used quantify mixing times to understand the interplay of mixing and chemical kinetics. The Bourne reactions are a great example in characterizing a reaction network and how the convolution of reaction kinetics with physical rate processes affects selectivity.

Johnson and Prud'homme [44] along with Mahajan and Kirwan [45] and Singh and coworkers [46] have used such reaction systems to characterize different mixing geometries to enhance mixing efficiency and reduce mixing times. A detailed description of the mixing characteristics and mechanisms is outside the scope of the present chapter, but rather the convolution of mixing with reaction kinetics will be discussed. This can be understood in the context of the fourth Bourne reaction as shown in Scheme 7.11.

The rate constants for k_1 and k_2 are $1.4 \times 10^8\ \mathrm{m^3/(mol\ s)}$ and $0.6\ \mathrm{m^3/(mol\ s)}$, respectively. The extent to which MeOH (or acetone) is observed in the final stream is indicative of poor mixing. A plot of conversion of the slow reaction to Damkohler number, that is, reaction to mixing time, is shown in Figure 7.13 for conducting the process in a mixing elbow in which the two process streams containing 2,2-dimethoxypropane and NaOH were mixed with HCl in a 180° angle. The details of the formulation of the mixing time and Damkohler number can be found elsewhere [46]. It is interesting to note that in spite of 8 orders of magnitude difference in rate, significant conversion of the slow reaction to methanol is observed. The reaction time constant defined as follows

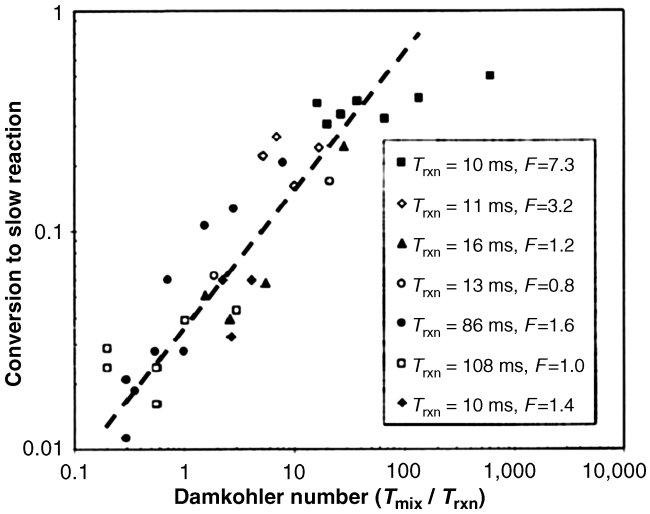

FIGURE 7.13 Plot of conversion of the 2,2-dimethoxypropane hydrolysis as a function of Damkohler number for time constants varying from 10 ms to 108 ms. *Source*: Ref. 46.

$$\tau_{rxn} = \frac{1}{k_2 C_0} \tag{7.17}$$

where k_2 and C_0 are the rate constant for the 2.2-dimethoxypropane hydrolysis and the concentration of the HCl in the final process stream, respectively. The reaction time constant was varied by 1 order of magnitude from 10 ms to 108 ms and the corresponding conversion to the slow reaction varied from 0.6 to 0.02. This application highlights the importance of understanding the convolution of physical processing parameters with reaction kinetics. Parameterization of the reaction kinetics allowed determination of the Damkohler number and developing a rationale for the significant changes in product distribution as a result of changes in operating parameters.

One of the challenges associated with scale-up is to determine whether liquid–liquid mixing under miscible conditions would be rate limiting and the effect on reaction rate and impurity formation. This is no trivial task and a number of diagnostic tests can be conducted, depending on the relevant reaction kinetics, to determine potential impact of mixing. Measurement of the rates of relevant chemical pathways (desired and undesired reactions) and comparison to the mixing timescales whether macromixing (bulk blending) or meso/micromixing. Correlations for mixing times under different mixing regimes for macro/meso/micromixing regimes have been articulated in the literature and will not be repeated in this report. Use of the Damkohler number type approach offers guidance on determining the effect of mixing on reaction performance.

Alternatively, one can also look at addition mode. Consider a case in which a stream of A is added to a stream of B to yield product C. Alternatively A and B could react to form D as shown in the scheme below

$$A + B \rightarrow C$$

$$A + B \rightarrow D$$

If the reverse addition is conducted, that is, a stream of B is added to a tank containing A, and no effect on rate on impurity formation is observed then one can fairly confidently conclude that mixing effects will be negligible. This is because the two addition modes mimic conditions in which you have either segregated high concentrations of A or B that would result from poor mixing at larger scales.

In contrast, if the order in B for formation of species C is greater than that for formation of D then the two different addition modes would give different ratios of species C and D; and hence mixing effects could potentially be pronounced at scale. There are several ways to manage the resulting mixing effect. Use of static mixers or auxiliary rapid mixing devices such as mixing elbows and vortex mixers can be used to enhance mixing while leaving the reaction kinetics unaffected thereby shifting the Damkohler number in the desirable direction. In contrast, the reaction kinetics itself can be slowed by either using dilution effects and taking advantage of differences in reaction order or temperature and leveraging the exponential dependence of temperature and/or differences in activation energy between the different chemical pathways.

7.7 GAS–LIQUID TRANSPORT

Gas–liquid mixing plays a central role in a number of commercialized synthetic processes. Transport of gas both into and out of solutions can drive reaction rates and selectivity.

One of the important issues that often arises when looking at gas–liquid phase reactions is the effect of solubility on reaction kinetics. In the presence of mass transfer limitations, gas solubility is clearly the driving force. However, the question of whether gas solubility affects reaction kinetics under conditions free of transport limitations can be more complex. Under ideal conditions, for multiphase reaction systems, that is, hydrogenations, the driving force, in the absence of transport limitations, is partial pressure of hydrogen and the rate in different solvents with varying hydrogen solubility would be independent of hydrogen solubility. There are unique situations in which nonidealities and interactions with the solvent can affect the driving force in a manner that hydrogen concentration becomes the driving force [24, 47, 48]. In the context of these results, care must be exercised when characterizing heterogeneous reaction system to ensure that the appropriate driving force is identified and used in the rate expressions.

A procedure for measuring the rate of mass transfer from the gas to liquid phases has been detailed previously [49]. The integral approach for measuring $k_L a$ is shown in the following equation:

$$k_L a \times t = \frac{P_f - P_o}{P_i - P_o} \ln \frac{P_i - P_f}{P - P_f} \tag{7.18}$$

where P_o, P_f, P_i, and P are solvent vapor pressure, final pressure, initial pressure, and pressure at a given time during the course of the experiment. Plotting the left-hand side of the above equation versus time yields a slope with units of 1/time; and it represents the mass transfer constant from gas phase to liquid phase. Alternatively, the initial slope of the pressure drop at the start of an uptake experiment to estimate the value of $k_L a$

$$k_L a \approx -\frac{dP}{dt} \frac{1}{P_i - P_f} \tag{7.19}$$

Note that for both large and small-scale measurements, it is important separately to understand the ramp up time for an agitator to reach full power. Experimental details for

measuring k_La and factors that affect gas–liquid mixing efficiency have been captured elsewhere and will not be repeated here [50].

As was the case for solid–liquid, liquid–liquid systems, the convolution of reaction rate with mass transfer from gas phase to liquid phase can be described using the Damkohler number is defined in equation 7.20.

$$Da = \frac{R_{\text{rxn}}}{R_{\text{MT}}^{\max}} = \frac{R_{\text{rxn}}}{k_La \times C_{\text{H}_2}^{\text{sat}}} \tag{7.20}$$

where R_{rxn} is the intrinsic reaction rate and $R_{\text{MT}}^{\max}$ is the maximum rate of transfer from the gas phase to the liquid phase. A ratio of $Da > 1$ is indicative of mass transfer limitations whereas $Da < 0.1$ is indicative of a regime *free* of mass transport limitations.

Understanding of $k_{\text{L}}a$ is critical to understanding and characterizing reactions involving gas–liquid mixing. This has been routinely shown in earlier work of Sun and coworkers. One particularly effective case study was the enantioselective reduction over supported Pd catalysts as shown in Scheme 7.5. Results are plotted in Figure 7.14. The maximum rate of mass transfer was varied from 0.0035 mol/(L min) to 0.51 mol/(L min) resulting in ee varying from 24% to 60%. The maximum rate of mass transfer could be varied by either changing the rate of mass transfer, that is, k_La, at a given pressure or by changing hydrogen solubility through changing the pressure at a given stirring speed and mass transfer constant. The filled circles in Figure 7.14 were obtained with varying stirring speeds but at a constant pressure [51]. Manipulation of pressure at a constant stirring speed of 750 rpm was effectively able to mimic the trend observed by changing stirring speed at a constant pressure.

The discussion above pertains primarily for mass transfer from gas phase to liquid phase. Similar issues are encountered when gas is desorbed off from liquid phase to gas phase. This issue is routinely encountered during oxygen sensitive reactions such as asymmetric hydrogenations and cross couplings in which trace concentrations of oxygen can poison catalysts or decarboxylation reactions in which effective desorption of CO_2 is necessary prior to forward processing. Similar issues are also encountered when the desired chemical transformation is an equilibrium in which a gas, that is, CO_2 or HCl, is produced along with the product and efficient removal of the gas from the liquid phase is necessary to push the desired reaction forward to completion. Phenomenologically, this reaction network can be described as follows:

$$\text{A} + \text{B} \Longleftrightarrow \text{C} + \text{HCl (l)}$$

$$\text{HCl (l)} \Longleftrightarrow \text{HCl (g)}$$

The formulation of the fundamental rate expression that describes this driving force is similar to that for the rate of transfer from gas phase to liquid phase. Specifically, the rate can be described as follows:

$$\text{Desorption rate} = \frac{dC}{dt} = k_{\text{L}}a(C - C^*) \tag{7.21}$$

where C is the solution phase concentration of the gas at a given time and C^* is the equilibrium concentration of the gas described by Henry's law. It must be noted that the k_La describing the desorption rate constant is different from that for absorption processes. Depending on the measurement approach, the value of C^* may vary during the measurement process; and additional mass balance in the gas phase would be necessary. As before, a detailed account of the mechanism of transport from solution to gas phase is outside the scope of the present report. Rather, the convolution of this transport process with reaction kinetics is often encountered.

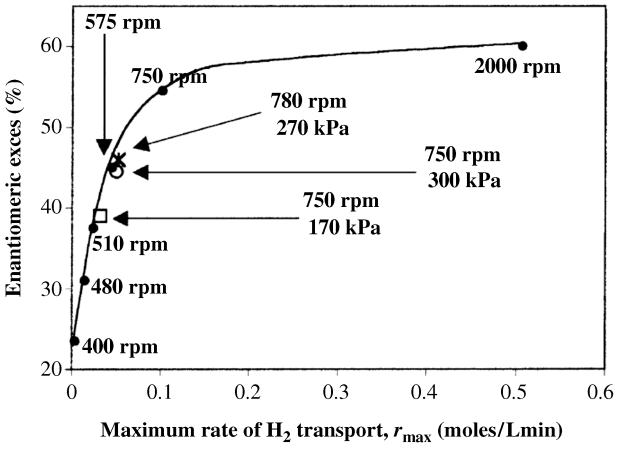

FIGURE 7.14 Effect of maximum rate of mass transfer on the final ee observed during enantioselective hydrogenation of supported Pd catalysts. *Source*: Ref. 24.

7.8 LEVERAGING THE ADVANTAGES OF CONTINUOUS REACTORS

Batch operating mode offers great flexibility in use of equipment, but can pose risks to successful scale-up. The most typical case of continuous reactors offering an advantage over batch operating conditions is for fast reactions with consecutive reactions that lead to "over-reaction." This is the case for either reactions that involve a reaction pathway with series of elementary reactions, or reactions in both series and parallel, and where the desired species is an intermediate [5]. This is the case for "unstable" reactions in quite a few instances in the pharmaceutical chemistry. Operating an unmixed (plug flow) continuous reactor or a continuous stirred reactor can offer advantages when such reactions are involved. In most other cases, batch reaction kinetics and that

TABLE 7.3 Opportunities for Continuous Reactions

Characteristic	Batch (8000 L Stirred Vessel)	Continuous (1 in. Pipe Reactor)	Advantage
Mixing time	>10 s (bulk blending)	>0.1 s	Rapid blending of reagents for fast reactions
Surface to volume available for heat transfer	$\sim 2\,m^{-1}$	$\sim 200\,m^{-1}$	Superior temperature uniformity with fewer "hot spots"
Typical temperature or pressure limit in absence of special designs	150°C; 10 Bar	200–250°C; 30–150 Bar	Ease of running reactions above the normal boiling point of solvents. Higher concentrations of gaseous reagents dissolved
Instantaneous amount reacting	100–1000 kg	1–5 kg	Lower energy potential and impact from runaway reaction

for plug flow reactions are identical when using the same conditions [5]. The use of continuous operation allows higher productivity than batch operating mode, but at the cost of more complex, less flexible, and capital intensive factories [52]. A list of general advantages is shown in Table 7.3.

The literature of the past 10–15 years has many instances of microreactors being investigated for the ability to improve performance, and highlighting issues such as those in Table 7.3, along with the ability to eliminate scale up by buying multiple reactor units. This sometimes includes a direct improvement, and other times involve subtle changes to the chemistry (Watts, Seeburger, and Jensen). Microreactors, such as larger scale continuous reactors, offer benefits in mixing and residence time control. At the same time, they present risks such as plugging that are not of the same level encountered in larger continuous reactors. They do offer great opportunity for lab-scale evaluation of rapid chemistry. The choice of whether to scale up in microreactors or traditional continuous reactors is linked to multiple considerations of economics that are beyond the scope of this effort.

Below, we present two industrial cases of using a continuous approach, one with a plug flow (unmixed) reactor and the second involving a stirred reactor.

In the original process to make imipenem, a desired inversion center in the backbone of the molecule was formed through a Mitsunobu inversion reaction followed by hydrolysis. Scheme 7.12 shows the original chemistry, which relied on hydrolysis under acidic conditions following the Mitsunobu inversion.

Because the inversion was carried out in water immiscible dichloromethane, the acidic hydrolysis required the addition of an equal volume of methanol prior to the addition of aqueous HCl. If scaled up directly, this would become a severe bottleneck to the volumetric productivity in manufacturing (Figure 7.15). The baseline yield for the inversion and hydrolysis was 80%, with the resulting intermediate **11** having a typical purity of about 99%. Importantly, the inversion and hydrolysis required over 40 L solvent per kilogram of **9**, and required significant use of water washing to remove methanol, then distillation to concentrate and dry **11** in DCM prior to crystallization.

Hence, hydrolysis at basic pH was investigated at lab scale as an alternative. In this case, intermediate **11** would be extracted into the aqueous phase as a sodium enolate. Batch experiments showed that the hydrolysis of the formate was feasible under basic conditions, but identified several challenges for successful processing. First, the hydrolysis was complete in less than 15 s. Second, the reaction tolerated up to 5 equiv of base, but only under cold conditions. Third, the beta-lactam began to undergo significant hydrolysis and ring opening after about 5 min of exposure to caustic. Fourth, the high solids loading prevented rapid (5 min) separation of the phases even at lab scale. Finally, neutralizing the excess

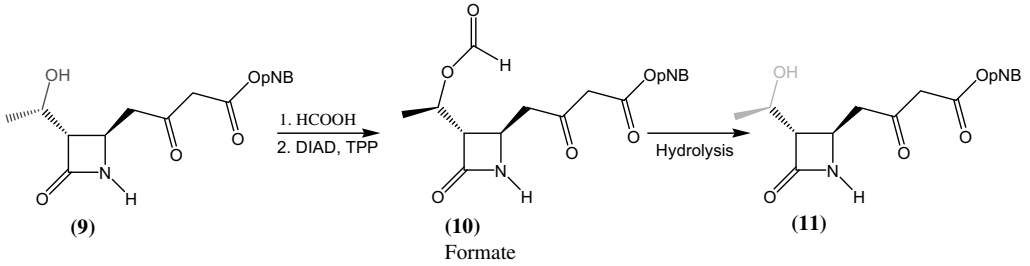

SCHEME 7.12 Extractive hydrolysis. *Source*: Ref. 53.

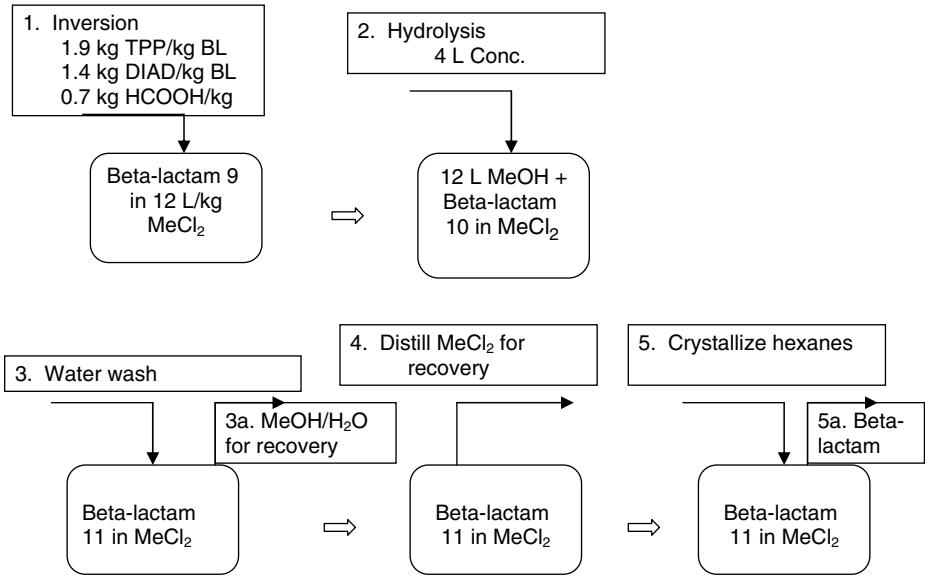

FIGURE 7.15 Flow sheet for acidic hydrolysis.

base prior to phase separation resulted in partitioning of **11** and spent reagents into the organic phase. This meant a very impure stream for crystallization.

From a reaction point of view, it was important to understand that the characteristic reaction time from laboratory studies indicated a half-life of no more than a few seconds, far less than the mixing time in a large stirred vessel. While the desired hydrolysis could be done in a stirred vessel, the half-life for degradation was not sufficiently longer than the mixing and batch wise phase separation time. So, scale-up in a batch process would result in 10–20% degradation by beta-lactam hydrolysis.

Thus, the poor separation required the use of enhanced separation of the liquid phases, and a centrifugal extractor was used to achieve the separation with a short contact time. In this case, the complete hydrolysis was straightforward, and the challenge became achieving a residence time and successful separation of spent reagents from **11** prior to neutralizing excess caustic. The equipment configuration ultimately implemented into the manufacturing process is shown in Figure 7.16.

This design implemented a rapid reaction of cold caustic with **10** followed by rapid separation and washing of the phases prior to neutralization. The productivity was more than 2.5 times that of the acidic hydrolysis route, exceeding the original goal. In addition, the yield was improved from 80% to more than 90%.

A second example is shown in Scheme 7.13, for the formation of an epoxide ring from an iodohydrin [53].

Initial batch experiments showed the reaction to take place very quickly, but require an excess of base to drive the reaction to completion, as seen in Figure 7.17.

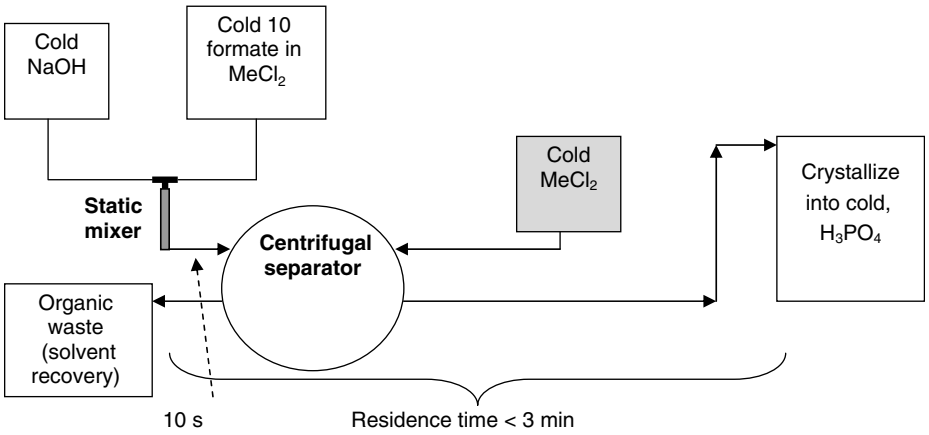

FIGURE 7.16 Flow sheet for continuous hydrolysis of **10** from Figure 7.15.

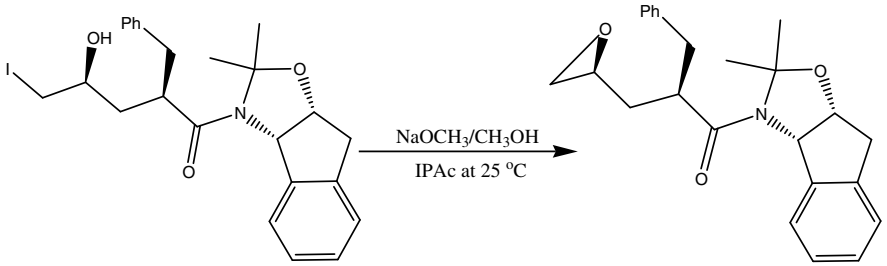

SCHEME 7.13 Epoxide formation from iodohydrin.

In this case, it was observed from batch experiments that back reaction could take place over several hours if sodium iodide remained in the reaction (Figure 7.18), and was sensitive to the pH. In particular, quenching the reaction only by adding water or IPAc would leave the resulting pH high and lead to enhanced back reaction, while neutralizing excess base would slow the back reaction kinetics.

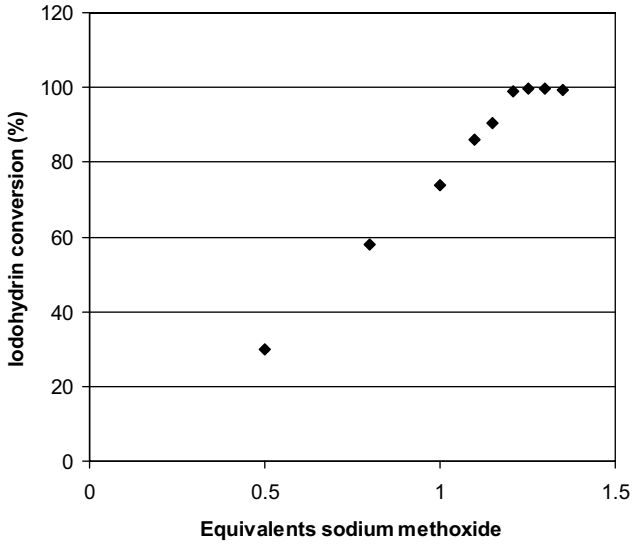

FIGURE 7.17 Impact of base charge on conversion in a "titration" experiment.

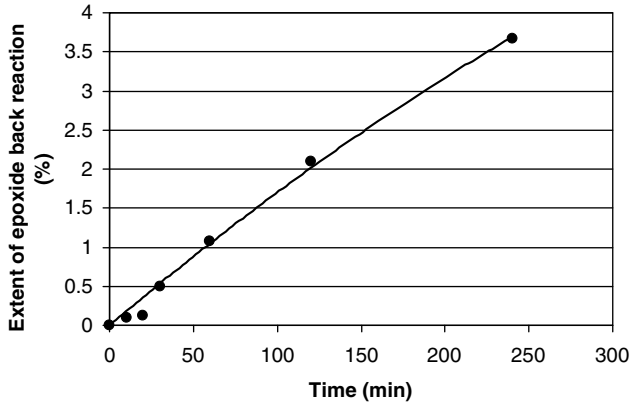

FIGURE 7.18 Extent of back reaction of epoxide to iodohydrin in an unquenched batch experiment (1.25 equiv of base).

Hence, it was desirable to limit the reaction time and exposure to basic conditions to avoid this reverse reaction. In order to avoid a loss of volumetric productivity that would accompany significant dilution to reduce back reaction, pH control would be desirable. This pH control also helped to minimize base catalyzed hydrolysis of IPAc by minimizing the exposure time of solvent at high pH. And finally, the neutralized salt layer was removed continuously from organic layer. Thus, the final process design was based on a continuous stirred reactor (CSTR) for the epoxidation followed by a CSTR with pH control to quench the excess base to prevent back reaction, and continuous separation of the aqueous phase to remove the aqueous salt layer (Figure 7.18). In addition to minimizing the risk and extent of back reaction, the short contact time also minimized IPAc hydrolysis, which improved yield in the solvent recycle step.

Today, there are many tools available to characterize such fast reactions at small scale, including stopped flow devices, microreactors and analytical technology such as described earlier in this chapter. All of this is useful to help characterize faster reactions in order to quantitatively understand the reaction timescale relative to that of mixing or transport rates of solids, gases, or even liquids to the reaction. As pointed out in Sections 7.5, 7.6, and 7.7, it is essential to quantitatively determine the timescale for reaction relative to the necessary mass or energy transport at every scale. Only this knowledge assures the process development expert that the chemistry is truly operating under the same limitations at each scale of operation, and with every equipment change.

7.9 CONCLUSIONS

In summary, the examples outlined above highlight the importance of understanding the interplay of chemical transformations with the physical rate processes, that is, heat and mass transfer resistances. Investigation of reaction kinetics and understanding of the elementary reactions in the pathway as well as quantification of the transport resistances is critical for ensuring successful process development and commercial scale-up and manufacture.

7.10 QUESTIONS

1. Derive the expression for k_la (gas–liquid). The mass transfer from the gas phase to the liquid phase can be described as shown below:

$$\text{Rate} = \frac{dC}{dt} = k_\text{L}a(C_t - C_\text{sat})$$

where C_t is the solution phase concentration of the gas at a given time and C_sat is the equilibrium concentration of the gas in solution. Integrating the above expression yield the following expression

$$\ln\left[\frac{(C_t - C_\text{sat})}{(C_0 - C_\text{sat})}\right] = \ln\left[\frac{(n_t - n_\text{sat})}{(n_0 - n_\text{sat})}\right] = k_\text{L}a \times t$$

where C_0 is the concentration of the gas in solution at $t = 0$ and n_0, n_t, and n_sat are the moles of gas initially in solution, moles of gas in solution at a given time t, and the moles of gas in solution at the saturation point. Mass balance for the gas yields the following:

$$n_t = n_0 + (P_0 - P_t)\frac{V_g}{RT}$$

$$n_\text{sat} = n_0 + (P_0 - P_f)\frac{V_g}{RT}$$

Substitution of the mass balance equation above yields the following expression for $k_\text{L}a$:

$$k_\text{L}a \times t = \ln\frac{P_f - P_t}{P_f - P_0}$$

2. For a reaction with a first order rate law, develop a rate expression that integrates the mass transfer constant for transport across the solid–liquid interface and the intrinsic reaction kinetics.
The rate of diffusion across the boundary layer is defined as follows:

$$R_\text{diff} = k_\text{d}(C_\infty - C_\text{I})$$

where C_∞ and C_I are the bulk and interface concentrations, respectively. The reaction rate for a power law rate model can be described as follows:

$$R_\text{rxn} = k_\text{r}C_\text{I}$$

Equating the above two expressions and solving for C_I yields the following expression:

$$C_\text{I} = \frac{k_\text{r}k_\text{d}}{k_\text{r} + k_\text{d}}C_\infty$$

Substitution of this expression into the equation for R_rxn yields the following:

$$R_\text{rxn} = \frac{k_\text{r}k_\text{d}}{k_\text{r} + k_\text{d}}C_\infty$$

REFERENCES

1. March J. *Advanced Organic Chemistry: Reactions, Mechanisms, and Structure*, 4th edition, Wiley, New York, 1992.
2. Rylander PN. *Hydrogenation Methods (Best Synthetic Methods)*, Academic Press, New York, 1985.
3. Astarita G. *Mass Transfer with Chemical Reaction*, Elsevier, Amsterdam, 1967.
4. Dankwerts PV. *Gas–Liquid Reactions*, McGraw-Hill, New York, 1970.
5. Levenspiel O. *Chemical Reaction Engineering*, 2nd edition, Wiley, New York, 1972.
6. Froment GF, Bischoff KB. *Chemical Reactor Analysis and Design*, Wiley, New York, 1979.
7. Dugger RW, Ragan JA, Ripin DHB. *Org. Process Res. Dev.* 2005;9:253–258.
8. Roberge DM. *Org. Process Res. Dev.* 2004;8:1049–1053.
9. Blackmond DG, *Angew. Chem. Int. Ed.* 2005;44:4302–4320.
10. Mathew JS, Klussmann M, Iwamura H, Valera F, Futran A, Emanuelsson EAC, Blackmond DG. *J. Org. Chem.* 2005;71:4711–4722.
11. Shekhar S, Ryberg P, Hartwig JF, Mathew JS, Blackmond DG, Strieter ER, Buchwald SL. *J. Am. Chem. Soc.* 2006;128:3584–3591.
12. Singh UK, Strieter ER, Blackmond DG, Buchwald SL. *J. Am. Chem. Soc.* 2002;124:14104–14114.
13. Boddington T, Chia HA, Halford-Maw P, Hongtu F, Laye PG. *Thermochim. Acta.* 1992;195:365–372.
14. Zogg A, Fischer U, Hungerbuhler K. *Indus. Eng. Chem. Res.* 2003;42:767–776.
15. LeBlond C, Wang J, Larsen R, Orella C, Sun Y-K. *Top. Catal.* 1998;5:149–158.
16. Stoessel F. *Thermal Safety of Chemical Processes: Risk Assessment and Process Design*, Wiley-VCH Verlag GmbH, Weinheim, 2008.
17. Munson J, Stanfield CF, Gujral B. *Curr. Pharmaceut. Anal.* 2006;2:405–414.
18. Schafer WA, Hobbs S, Rehm J, Rakestraw DA, Orella C, McLaughlin M, Zhihong G, Welch C. *Org. Process Res. Dev.* 2007;11:870–986.
19. Hughes D, Zhao D. *J. Org. Chem.* 1993;58:232.
20. Sun Y-K, Wang J, LeBlond C, Landau RN, Blackmond DG. *J. Catal.* 1996;161:759–765.
21. Lin SD, Vannice MA. *J. Catal.* 1993;143:539.
22. Lin SD, Vannice MA. *J. Catal.* 1993;143:563.
23. Singh UK, Vannice MA. *J. Catal.* 2000;191:165–180.
24. Singh UK, Vannice MA. *AIChE J.* 1999;5:1059.
25. Mears DE, Boudart M. *AIChE J.* 1966;12:313.
26. Vannice MA, Hyun SH, Kalpakci B, Liauh WC. *J. Catal.* 1979;56:358.
27. Boudart M. *AIChE J.* 1972;18:465.
28. Boudart M, Mears DE, Vannice MA. *Ind. Chim. Belge.* 1967;32:281.

29. Laidler KJ. *Chemical Kinetics*, 3rd edition, HarperCollins Publisher, New York, 1987, pp. 183–220.
30. Zwietering ThN. *Chem. Eng. Sci.* 1958;8:244.
31. Paul EL, Atiemo-Obeng VA, Kresta SM. *Handbook of Industrial Mixing: Science and Practice*, Wiley, Hoboken, NJ, 2004.
32. Pangarkar VE., Yawalkar AA., Sharma MM., Beenackers AACM. *Ind. Eng. Chem. Res.* 2002;41:4141–4167.
33. Barker JJ, Treybel RE. *AIChE J*. 1959;6 (2): 295.
34. Harriott P. *AIChE J*. 1962;8 (1): p101ff.
35. Harriott P. *AIChE J*. 1962;8 (1): p93ff.
36. Brian PLT, et al. *AIChE J*. 1969;15 (5): 727.
37. Davies JR. *Chem. Eng. Process.* 1986;20 (4): 175.
38. Marrone GM, Kirwan DJ. *AIChE J*. 1986;32 (3): 523.
39. Armenante PM, Kirwan DJ. *Chem. Eng. Sci.* 1989;44 (12): 2781.
40. Garside J, Mersmann A, Nyvlt J. *Measurement of Crystal Growth and Nucleation Rates*, 2nd edition, Institution of Chemical Engineers, U.K., 2002.
41. *Perry Chemical Engineering Handbook*, 8th edition, McGraw-Hill, New York, 2007, pp. 7–19.
42. Singh UK, Pietz MA, Kopach M. *Org. Process Res. Dev.* 2009;13:276–279.
43. Bourne JR. *Org. Process Res. Dev.* 2003;7:471–508.
44. Johnson BK, Prud'homme RK. *AIChE J*. 2003;49 (9): 2264–2282.
45. Mahajan AJ, Kirwan DJ. *AIChE J.*, 1996;42 (7): 1801–1814.
46. Singh UK, Spencer G, Osifchin R, Tabora J, Davidson OA, Orella C. *Ind. Eng. Chem. Res.* 2005;44:4068–4074.
47. Madon RJ, O'Connell JP, Boudart M. *AIChE J*. 1978;24:904.
48. Gonzo RE, Boudart M. *J. Catal.* 1978;52:462.
49. Demling A, Karandikar BM, Shah YT, Carr NL. *Chem. Eng. J*. 1984;29:140.
50. Oldshue JY. *Chem. Eng. Progr.* 1980;76 (6): 60.
51. Singh UK, Vannice MA. *Appl. Catal. A Gen.* 2001;213: 1–24.
52. Khurana A. *Sloan. Mgmt. Rev.* 1999; *Winter*.
53. King ML, Forman AL, Orella CJ, Pines SH. *Chem. Eng. Progress* 1985; May: 36–39.
54. Maligres PE, et al. *Tetrahedron* 1996;52 (9): 3327–3338.